Materials Science Forum
ISSN: 1662-9752, Vol. 1062, pp 263-267
doi:10.4028/p-oneqg9

Submitted: 2021-10-12
Revised: 2022-02-10
Accepted: 2022-04-20
Online: 2022-05-31

Phosphorous and Aluminum Implantation for MOSFET Manufacturing: Revisiting Implantation Dose Rate and Subsequent Surface Morphology

J. Woerle[1,a*], M. Belanche[1,b], M. Negri[2,c], C. Lamontagne[3,d], F. Bonafè[4,e], R. Nipoti[4,f], U. Grossner[1,g]

[1]Advanced Power Semiconductor Laboratory, ETH Zurich, Physikstrasse 3, 8092 Zurich, Switzerland

[2]Axcelis Technologies Srl, Agrate Brianza, Italy

[3]Axcelis Technologies Inc., Beverly, MA, USA

[4]CNR-IMM Bologna, via Gobetti 101, I-40129 Bologna, Italy

*[a]woerle@aps.ee.ethz.ch, [b]belanche@aps.ee.ethz.ch, [c]marco.negri@axcelis.com, [d]christopher.lamontagne@axcelis.com, [e]bonafe@bo.imm.cnr.it, [f]nipoti@bo.imm.cnr.it, [g]ulrike.grossner@ethz.ch

Keywords: Ion implantation, resistivity, thermal oxidation, oxidation rate.

Abstract. In this work, we study the impact of the dose rate on the electrical properties of aluminum (p-body, p^+-body-contact) and phosphorous (n-source/drain) implanted 4H-SiC. We find no significant differences for dose rates ranging from 1×10^{11} $cm^{-2}s^{-1}$ to $2–7\times10^{12}$ $cm^{-2}s^{-1}$. AFM scans across implanted and non-implanted regions after thermal oxidation and subsequent oxide etching reveal a clear dependence of the oxidation rate on the conduction type and doping concentration. In addition, we observe an increasing (decreasing) oxidation rate for increasing doping concentrations of the n-type (p-type) ion implanted areas.

Introduction

For many silicon carbide (SiC) based devices, selective doping by ion implantation is one of the most critical steps during the fabrication process. Undesired variations of the physical or electrical doping profile, increased lattice damage as well as modifications of the surface morphology after the activation annealing can have a significant impact on the final device performance [1-3]. Fortunately, many of the mentioned issues have already been studied in detail or are the focus of ongoing research; however, results are not always conclusive and can strongly depend on the sample preparation or technical details of the implantation and activation annealing process. Furthermore, ion implanters for research purposes may result in notable differences compared to industry-oriented implantation facilities where processes are often performed at much higher dose rates.

To address the open question of process reproducibility, we compare ion implantation and activation-annealing processes performed at two different implantation facilities and show that despite significant differences of the dose rate almost identical electrical properties may be achieved.

In the second part of this work, we focus on the oxidation properties of phosphorous and aluminum implanted SiC by performing an atomic-force microscopy (AFM) study of the surface morphology across the borders of ion-implanted areas and the non-implanted n-type epi-layer after thermal oxidation and subsequent oxide removal. In previous studies on heavily implanted or amorphous SiC [4,5], it was shown, that the lattice damage introduced during high-dose implantations resulted in enhanced oxidation rates, independent of the conduction type. In moderately doped SiC epitaxial layers, on the other hand, Kobayashi et al. [6] found a clear rate dependence both on the doping concentration and the conduction type with an increased oxide thickness for heavily doped n-type SiC and a reduced oxidation rate for p-type SiC. The authors explained their results by the presence of Si vacancies promoting surface reactions in the case of n-type SiC, as well as high densities of Al atoms in the oxide of heavily p-doped SiC, causing a deceleration of the oxide growth. Our AFM

analysis on implanted SiC confirms this trend; however, compared to epitaxial p-type SiC, in the case of Al-implanted SiC, the observed height variations after sacrificial oxidation are significantly higher.

Experimental Details

Within this study, we investigate phosphorous (P) and aluminum (Al) implantations on 4° off <0001> axis, low-doped n-type 4H-SiC. The implantation parameters were chosen to reflect typical doping densities used for the fabrication of lateral SiC MOSFETs. The multi-energy implantations were performed either at a HV Tandetron 1.7 MeV accelerator (Samples A and B) or an Axcelis Purion tool (Sample C) [7], resulting in an implantation profile as described in Table I. Details on the implantation and annealing parameters are given in Table I. After removal of the capping layer and a cleaning step including a 44 nm thick sacrificial oxide, a gate oxidation in O_2 at 1250 °C followed by annealing in NO was performed on Sample C. The final gate oxide thickness was 45 nm. The oxide thickness on the non-implanted areas has been estimated by ellipsometry measurements. For the electrical analysis, Van-der-Pauw structures were fabricated for which either Ni or Ti/Al were used for ohmic contacts on the P and Al ion implanted areas, respectively.

Table I. Sample parameters for the ion implantation and subsequent activation annealing [8,9], where *d* is the depth of the ion implanted region, T_{impl} and T_{ann} are ion implantation and post implantation annealing temperature, respectively, and t_{ann} post-implantation annealing time.

Sample name	Implantation type	Impl. density (cm^{-3})	*d* (nm)	Dose rate ($cm^{-2}s^{-1}$)	T_{impl} (°C)	T_{ann} (°C)	t_{ann} (min)
A	P, n^+ Al, p-body Al, p^+	5.4×10^{18} 3×10^{18} 7.9×10^{18}	240 250 195	1×10^{11}	400 430 430	1600	30
B	P, n^+ Al, p-body Al, p^+	5.9×10^{18} 3×10^{18} 8.5×10^{18}	344 242 312	1×10^{11}	400 430 430	1600	300
C	P, n^+ Al, p-body Al, p^+	$3\text{-}5\times10^{18}$ 3×10^{18} 7×10^{18}	190 240 220	7×10^{12} 2×10^{12} 4×10^{12}	500	1700	30

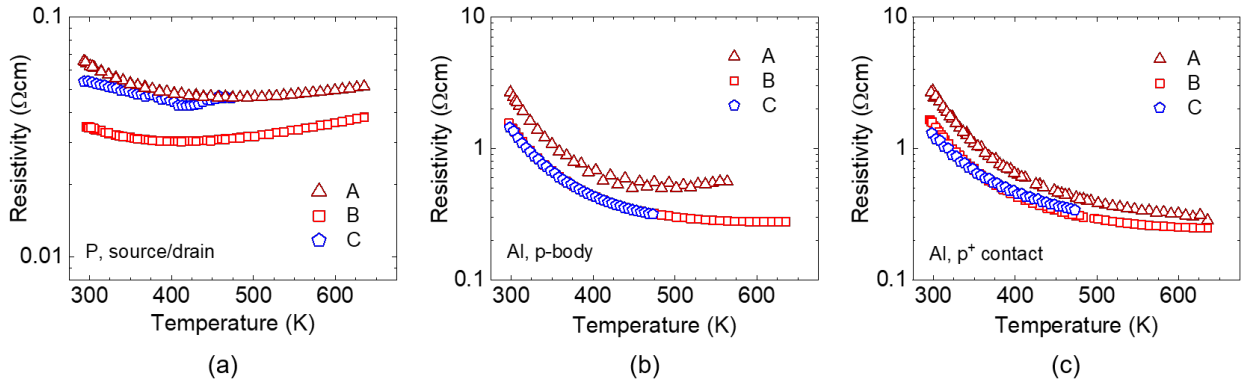

Fig. 1. Resistivity measurements extracted from Van-der-Pauw structures in the temperature range from 300 K to 650 K. (a) P implantation for source/drain, (b) Al implantation for the p-body, (c) Al implantation for the p^+-body-contact.

Electrical Characterization

In Fig. 1, the resistivity of source/drain (Fig. 1(a)), p-body (Fig. 1(b)), and p-body-contact (Fig. 1(c)) ion implanted layers for different dose rates during the implantation are compared. All curves show a negative temperature coefficient at low temperatures, which is more pronounced for the Al implantations. In agreement with previous reports [10], the resistivity decreases with increasing annealing time or annealing temperature. Despite the large differences in dose rate - 20 to 70 times larger in Sample C than in Samples A and B - very similar resistivity values between the samples are observed for both the dopants. This result highlights the possibility of reproducing studies performed on research facilities often using low dose rates in the context of industrial processing.

AFM Characterization

In a next step, modifications of the surface morphology due to thermal oxidation were studied. In addition to changes of the surface morphology introduced during activation annealing [11], also subsequent processing steps such as thermal oxidation may significantly alter the surface roughness. When growing an SiO_2 layer by thermal oxidation, a SiC layer of around 46% of the oxide thickness is consumed. As the oxidation rate of epitaxial SiC shows a clear dependence on the doping sign and on the doping density [6], variations of the final oxide thickness and hence SiC consumption may be expected between ion-implanted and non-implanted regions undergoing the same oxidation process. Due to this variation in oxidation rate, the surface morphology across differently implanted areas may offer an estimation of the local oxide thickness on the differently ion implanted regions. Fig. 2 summarizes the results of this oxidation-induced step formation for sample C: compared to non-implanted regions, the n-type implantation (P density: $\sim 4\times10^{18}$ cm^{-3}) exhibits an increased SiC consumption of around 7.5 nm, while both p-type implanted regions show less consumption of the SiC with height differences of 1.2 nm and 6.0 nm. For these Al-implanted areas, the reduction of the oxide growth rate is more pronounced for larger doping concentrations. Based on our results, a schematic drawing of the surface of a double-implanted MOSFET after thermal oxidation is depicted in Fig. 2(e).

The increased oxidation rate on n^+ ion-implanted SiC with respect to n^- epitaxial SiC may be due to the sum of two effects, both enhancing the oxidation rate: enhanced surface reactions caused by Si vacancies [6], as well as the presence of lattice disorder even after the high temperature post implantation annealing [5]. However, when comparing our findings to the Deal-Grove model on epitaxially grown SiC [6] we find excellent agreement, suggesting no or only a minor contribution of lattice damage to the increased oxidation rate in ion implanted n-type regions.

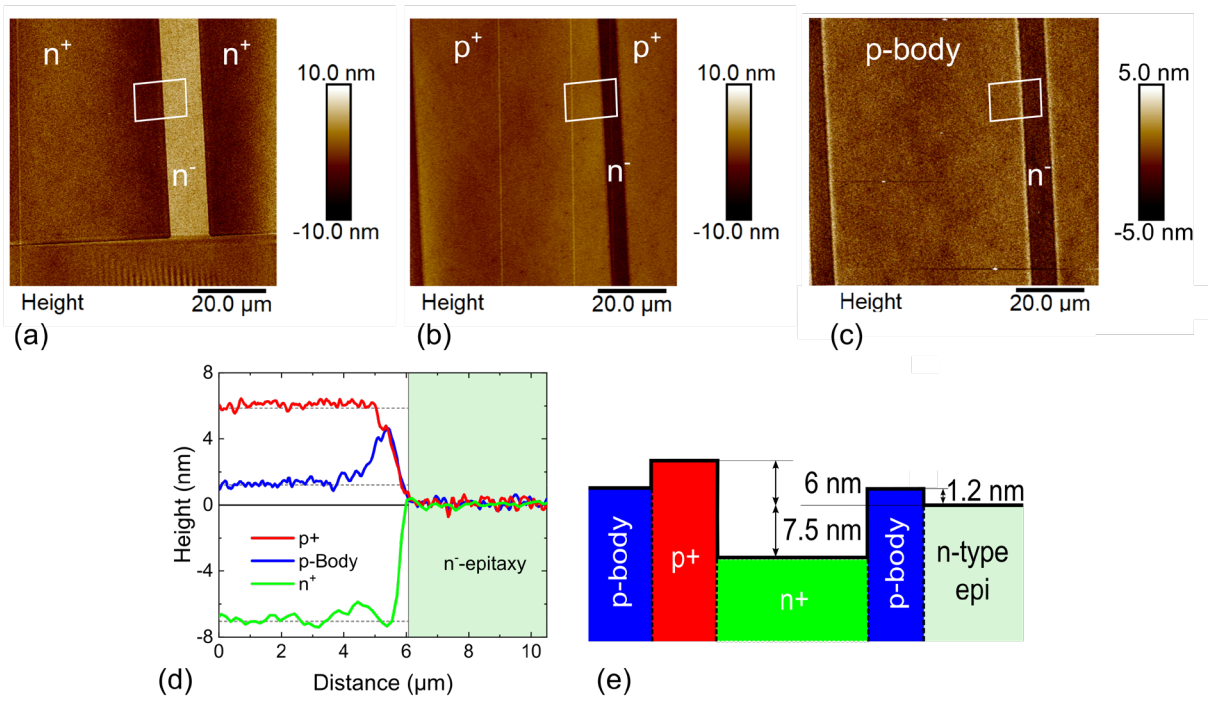

Fig. 2. (a,b,c) AFM height maps of the SiC surface after oxide removal. (d) Corresponding height profiles extracted from the areas indicated in (a,b,c). Note the differences in scale. (e) Summary of all measured height differences with respect to the n-type epi region.

In the case of Al implanted SiC, we observe a stronger reduction of the oxide growth rate compared to epitaxial p-type SiC: there, considering a similar doping concentration and oxide thickness, height differences around 0.5 nm compared to low-doped n-type or p-type SiC would be expected [6]. This discrepancy is unlikely to be the result of lattice damage in the annealed ion-implanted layer as this would lead to an enhanced growth rate. Instead, we tentatively attribute the reduced oxide growth for the Al-implanted regions to Al atoms from the consumed SiC: being trapped in the oxide the Al may hamper the O_2 diffusion from the surface towards the oxide/SiC interface where new oxide is formed.

Another interesting feature of Fig. 2(d) is the peak between the p-body and the n^- epi-layer showing an intermediate region with a reduced SiC consumption compared to the p-body region. In the light of our previous discussion, such a peak may be justified by a local increase in the Al lateral depth profile. In fact, the simulation of the two-dimensional ion depth distribution at a mask border suggests a higher density of the implanted species along the lateral depth profile immediately below the mask border [12]. A similar increased concentration of the implanted dopant under mask border takes place in the case of the p^+ and n^+ implantations. The fact neither a peak nor a depletion are visible across the borders of the p^+/n^- or the n^+/ n^- regions may be attributed to a less pronounced variation of the oxidation rate at elevated doping densities [6].

Conclusion

In this study, we compared ion implantation processes, which were performed at dose rates between 1×10^{11} $cm^{-2}s^{-1}$ and 7×10^{12} $cm^{-2}s^{-1}$ and find no significant difference in the resistivity values of the implanted areas. A subsequent AFM analysis of the SiC consumption during thermal oxidation across the implanted regions reveals height differences of up to 13.5 nm, suggesting a more pronounced doping dependence than what has been reported previously for epitaxial p-type and n-type SiC. Future work will focus on understanding the exact mechanism of the strong reduction of the oxidation rate for Al-implanted SiC as well as to improve the understanding of mask-related height variations observed at the edges of the implanted areas.

Acknowledgements

We thank Mr. Fabrizio Tamarri and Mr. Michele Sanmartin for their help with sample processing at the CNR-IMM clean room facilities. The ETH Zurich Foundation is gratefully acknowledged for their financial support.

References

[1] T. Dalibor et al., Phys. stat. sol. (a) 162, 199 (1997).

[2] R. Nipoti et al., Mater. Sci. Semicond. Process. 78, 13-21 (2018).

[3] M. A. Capano et al., J. Electron. Mater. 28, 214 (1999).

[4] K. Ueno, and Y. Seki, Jpn. J. Appl. Phys. 33, 1121 (1994)

[5] A. Makhtari, V. Raineri, F. La Via, G. Franzó, F. Frisina, and L. Calcagno, Mater. Sci. Semicond. Process. 4, 345-349 (2001).

[6] T. Kobayashi, J. Suda, and T. Kimoto, Appl. Phys. Express 7, 121301 (2014).

[7] Information on https://www.axcelis.com/.

[8] R. Nipoti et. al., Mat. Sc. Forum 1004, 698-704 (2020)

[9] R. Nipoti et. al., Mat. Sc. Forum 1004, 683-689 (2020)

[10] P. Fedeli et al., ECS J. Solid State Sci. Technol. 5 (9), P534-P539 (2016).

[11] M. Canino et al., J. Microsc. 280, 229-240 (2020).

[12] G. Lulli, IEEE Trans. Electron. Devices **58**, 1 (2011).

The publication of this article was funded by the ETH Zurich 10.13039/501100003006